AI learns to forecast global flood events from historical news

Oleg Zlydenko[1,*], Hadas Fester[1], Shmuel Fronman[1], Martin Gauch[1], Oren Gilon[1], Avinatan Hassidim[1], Gila Loike[1], Yossi Matias[1], Rotem Mayo[1], Grey Nearing[1], Aviel Niego[1], Reuven Sayag[1], Shruti Verma[2], Ido Zemach[1], and Deborah Cohen[1]

[1]Google Research
[2]Jigsaw, work was done while at Google Research
[*]Corresponding author: olegzl@google.com

This is an unreviewed preprint

Abstract

The World Meteorological Organization estimates that over a third of countries lack flood forecasting systems or the hydrological data to develop such systems[1]. Even in regions equipped with streamflow gauge networks, these sensors primarily monitor main river channels and fail to capture rapid-onset flash, pluvial, and urban floods, which account for roughly 85% of global flooding cases[2]. Here we present an artificial intelligence system that overcomes this physical data barrier by learning to forecast flood events from unstructured news reports at a global scale. We distilled over 5 million historical news articles into a structured dataset with a Large Language Model, and trained a deep learning model to forecast these flood events up to a 24-hour lead time directly from weather patterns. Extensive spatial cross-validation demonstrates strong zero-shot generalization on areas encompassing 88% of the global population: in completely held-out countries, the model achieves state-of-the-art precision and recall, matching or exceeding localized physical expert systems from national warning agencies across diverse geographies. Currently operational in over 150 countries, this system demonstrates that shifting ground truth from physical sensors to human observation enables universal, off-network flood forecasting at a global scale.

Main

Between 2000 and 2019, floods affected over 1.6 billion people worldwide and caused nearly $650 billion in economic losses[3]. Early warning systems (EWS) set the foundation for global resilience against such disasters: providing just a 12-hour notice of impending rapid-onset flood events can cut the ensuing damage by 60%[4]. To maximize the effectiveness of these warnings, the global early warning community has embarked on a shift from traditional physical modeling to impact-based prediction. Led by the World Meteorological Organization (WMO) and the Sendai Framework, this new paradigm focuses on forecasting "what the weather will do" rather than "what the weather will be"[5,6,7].

However, realizing this socio-hydrological paradigm shift remains particularly challenging for rapid-onset, off-channel inundation[8]. These localized events account for roughly 85% of global flooding cases and cause massive annual losses in life and property[2,3,8]. While riverine inundation can be monitored by stream gauges, there is no equivalent physical variable to indicate off-channel flash, pluvial, or urban floods. High-resource, developed nations therefore employ rainfall thresholding approaches that rely on precise real-time observational data and local expert knowledge.

Consequently, the capacity to anticipate flood threats is deeply unequal across the world. Regions in the Global North use advanced systems such as the United States Flash Flood

Guidance (FFG)[9,10] or the European Runoff Index based on Climatology (ERIC)[11]. FFG calculates dynamic rainfall thresholds to exceed soil infiltration capacity, while ERIC simulates soil moisture and runoff using the LISFLOOD hydrological model[12] against a climatological baseline. These approaches rely heavily on dense physical sensor networks, high-resolution observations, and historical gauge data. Vast regions of the Global South lack this instrumentation, which creates a severe "warning gap"[7]: while Asia experienced 40% of all flood events between 2000 and 2019, it accounted for more than 90% of people affected by floods worldwide[3].

Overcoming this gap requires global forecasting systems that do not rely on local calibration or simulated water routing. To this end, we present a human impact-focused global flood event prediction system based on Artificial Intelligence (AI). We trained and evaluated the model on Groundsource[13], a structured dataset that the Large Language Model (LLM) Gemini[14] distilled from over 5 million unstructured news articles. By shifting the ground truth from physical sensors to human reports, our system skips physical quantities and directly predicts the occurrence of socio-hydrological flood events. To tightly couple physical hazards with human impacts, we explicitly mask our operational domain to populated areas (> 100 people per km^2), encompassing roughly 88% of the global population. This ensures that severe meteorological events inevitably intersect with infrastructure.

On the basis of the model and extensive experimental validation, we developed an operational system that produces up to 24-hour warnings about imminent flooding in more than 150 countries. These forecasts augment our existing riverine flood forecasts[15] and are openly available in real time at `https://g.co/floodhub`. In the remainder of this paper, we demonstrate that our approach generalizes effectively across diverse geographies and achieves predictive performance comparable to or exceeding state-of-the-art national warning systems.

AI flood event forecasts generalize in space

To evaluate the model's ability to generalize to unseen regions, we conducted a spatial cross-validation experiment with a focus on five diverse countries: the United States, Brazil, the United Kingdom, South Africa, and the Philippines (Figure 1a–e). These countries represent nations with sufficient Global Disaster Awareness and Coordination System (GDACS)[16] events from different continents, prioritizing countries that also possess publicly available alerts archives for the years 2021 to 2025.[1] For each country, we compared the precision–recall curve of the full AI model, where the country was included in the global training set, against a zero-shot AI model, where the country was strictly held out from training. The globally trained model achieves areas under the precision–recall curve (AUPRC) between 0.21 (evaluated in the Philippines) and 0.33 (Brazil). When a country is strictly held out from training, we observe only a moderate decrease in AUPRC, with the zero-shot models retaining between 70% (U.S.) and 90% (Philippines) of the globally trained model's AUPRC. The model therefore effectively learns generalizable physical and meteorological patterns, and does not merely memorize local geographical specifics. These per-country results are also largely representative of the full evaluation across the entire global coverage area. There, the model achieves an AUPRC of 0.23 (Figure 1f). At a classification threshold of 0.74, the global evaluation reaches its optimal F1 score of 0.30. Extended Data Table 3 details the exact sample sizes for all evaluations.

To contextualize these performance values, we compared the AI model performance against the baseline of local expert systems from the national warning agencies of the U.S., Brazil, and the U.K. (colored markers in Figure 1). The AI model achieves performance comparable to the expert systems in the U.S. and exceeds the quality of the warnings for the U.K. and Brazil. Evaluated at the optimal threshold of 0.74, the F1 scores of the global AI system are between 1.13 (U.S.) and 3.24 (Brazil) times higher than those of the corresponding local expert systems.

[1]We calculate recall on GDACS events to measure the model's ability to retrieve high-impact events. In Extended Data Figure 6, we reproduce a version of Figure 1 that calculates recall on Groundsource events.

Even the zero-shot spatial holdout models achieve comparable performance; the ratio of F1 scores between zero-shot model and local expert system ranges between 0.83 (U.S.) and 2.07 (Brazil). Extended Data Table 2 provides all absolute metric values, including additional Critical Success Index (CSI) scores. Further, Extended Data Figure 6 contains a full comparison against public alerts in Taiwan, where no GDACS data was available. Compared on Groundsource labels, the AI model predictions outperformed the local expert system in Taiwan, as well.

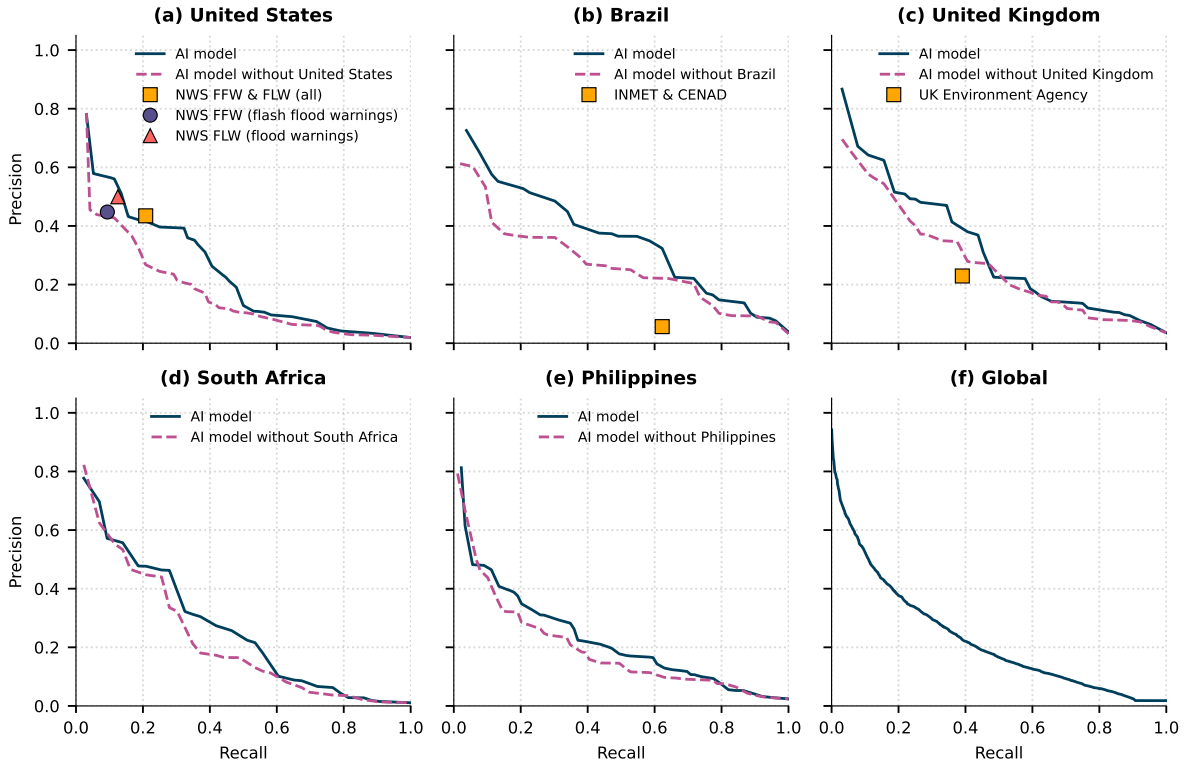

Figure 1: Per-country and global precision–recall evaluation. Each panel a–e displays the performance of the AI model when the evaluated country was included in the training data (solid blue line) versus when it was held out for zero-shot generalization (dashed pink line). The markers represent the baseline performance of respective national warning agencies for all countries except South Africa and the Philippines, where such data was unavailable. For the U.S., the square marker represents the performance of the combined Flood and Flash Flood Warnings. Panel f shows the performance across the full global area of coverage.

Because Groundsource was created by scraping often short-lived web pages for news articles, the dataset is skewed towards more recent events[13]: the years 2024 and 2025 are over-represented with around 53% of the total articles, while the longer period 2021–2023 comprises only 47%. In the evaluation, this skewness causes us to underestimate the model performance, especially in earlier years. As the AI model training employed a yearly cross-validation setting, we can dissect the performance over time and illustrate this effect in Figure 2: the earlier evaluation years (2021–2023) were trained on more, but evaluated on fewer events than the more recent years (2024–2025). Despite the smaller training dataset, the more recent evaluation years perform better than the earlier ones, as the more comprehensive Groundsource coverage reduces the number of cases where the model correctly predicts an event that is missing in Groundsource. As we continue to expand the Groundsource dataset in real-time based on newly appearing articles, we will no longer rely on historical articles still being available on the internet. Hence, this effect will gradually diminish in future evaluations.

To provide further detail from a spatial perspective, Figure 3 breaks down the precision and

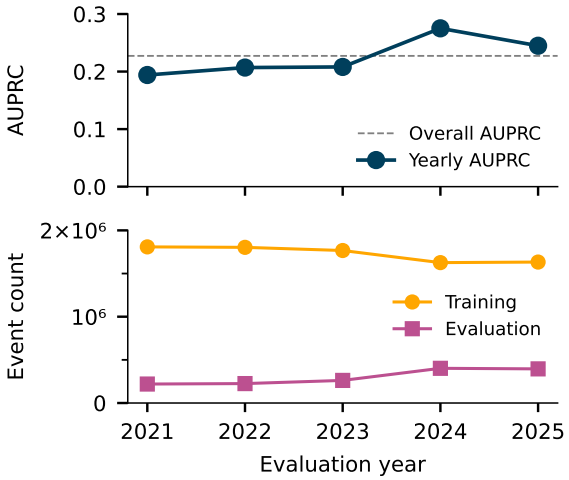

Figure 2: AUPRC (top) and training and evaluation event count (bottom) over time. The cross-validation folds that evaluate more recent years were trained on fewer, but evaluated on more events due to the recency bias in Groundsource. Still, the AUPRC metric values in recent years are higher, as precision is underestimated less. The dashed gray line in the upper plot shows the overall performance across all years for reference.

recall performance by country at the classification threshold of 0.74, which yields the best F1 score globally. The results for some countries in this regional analysis are inherently subject to greater uncertainty than others, because the amount of ground truth events in Groundsource and GDACS varies as indicated in the bottom row of Figure 3. We excluded countries with fewer than 10 ground truth events from our analysis to limit the resulting noise. Nevertheless, the precision values are homogeneous across most countries, with a mean of 0.22, 25th percentile of 0.14, and 75th percentile of 0.29. Central Africa and parts of the Middle East and Asia have lower precision, which we largely attribute to the limited representation of these regions in Groundsource. As illustrated in Figure 2, this lack in coverage causes us to underestimate precision, because positive predictions are treated as incorrect when a flood occurs, but no corresponding news report exists. In terms of recall, parts of South America and South-East Asia stand out with particularly high values. We hypothesize that this might be due to their exposure to tropical storms. Floods during these extreme events are relatively easy to predict and well-covered in the Groundsource training data, which results in more accurate warnings.

Conclusion and discussion

Traditional flood modeling based on explicit physical processes struggles to provide the flexibility necessary to represent complex and varied flood types, leaving a gap between model simulations and disaster warnings[17]. AI-based methods enable a shift towards an event prediction paradigm that puts the human impact front and center. By learning from a global ground truth dataset extracted from millions of unstructured news articles rather than calibrating against physical sensors, we have overcome a primary barrier to expanding early warning systems to populated regions anywhere on Earth. Even in zero-shot scenarios where local data is entirely withheld, the AI models yield globally consistent predictions with comparable or better accuracy than established local expert systems across diverse geographies.

In the future, we expect that improvements in global meteorological forecasting will increase the spatial resolution and consequently enhance localized precision. Additionally, LLMs will get better at classifying events and extracting spatiotemporal information, especially from reports

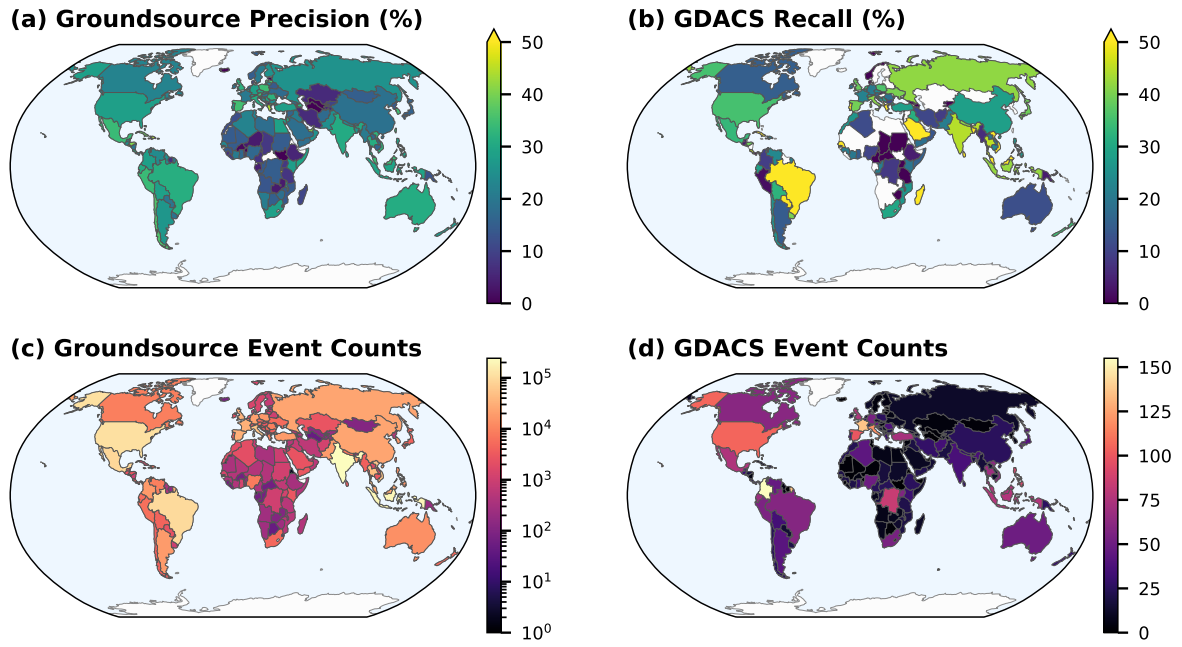

Figure 3: Map of precision (a), recall (b), event count according to Groundsource (c), and event count according to GDACS (d) by country. We excluded countries with less than 10 ground truth events from panels (a) and (b), as their metrics would be very noisy. For a clear visual display, we limited the precision and recall color scale to 50%.

in low-resource languages. These improvements directly translate into better training and evaluation data, which in turn benefit the forecasting system. Specifically, better Groundsource data will allow us to expand coverage and relax the current constraint of populated areas, but also to better distinguish different flood types. The most devastating urban disasters occur as compound events, driven by immediate local rainfall and broader riverine accumulation [18]. Therefore, coupling this impact-based system with predictions from established global riverine AI models promises to bridge the gap between localized meteorological triggers and basin-scale hydrological modeling.

At a broader scale, the methodology presented here—using Large Language Models to distill unstructured human reports into structured, spatiotemporal records, and then training AI models on those records—represents a generalizable template for the Earth sciences. We see potential to adapt this strategy for improved monitoring of other under-instrumented hazards such as the consequences of extreme heat, landslides, or avalanches, where human observations often outpace physical sensor coverage.

Methods

Our forecasting system uses a Long Short-Term Memory network (LSTM) [19], an architecture that has proven well-suited for environmental and especially hydrological time-series data [20,21]. Specifically, we build upon the work by Nearing et al., who developed a hydrological forecast model for riverine floods using LSTMs [15]. To capture localized, precipitation-driven inundation threats (as opposed to basin-scale river routing), we feed the model input data as pixels with a spatial resolution of $0.2° \times 0.2°$, with study regions cropped to land masses.[2] The spatial

[2]Cutting off non-landmass areas can cause irregular shapes, but for the sake of simplicity, we call the prediction areas "pixels" in this manuscript nevertheless.

resolution is primarily driven by the granularity of globally available atmospheric data. To improve the granularity of events after rasterization, we let adjacent pixels overlap by 0.1°.

The model integrates static geophysical properties with dynamic hourly meteorological data, detailed below. Specifically, it processes a 7-day hourly historical hindcast sequence followed by a 24-hour hourly forecast window. The model generates a score that represents the probability of a flood event occurring within the forecast window in the target region.

The architecture processes static attributes through a series of dense embedding layers to produce a fixed-length representation. Dynamic features are organized into discrete feature groups, by their provider, each of which is independently embedded to capture group-specific temporal dynamics. We handle missing data in the input streams with the masked mean architecture described in Gauch et al.[22]: a mechanism that ignores missing data points and calculates a mean across the embedded feature groups to aggregate information from valid inputs. This temporal summary is concatenated with the embedded static attributes at every time step and fed into the LSTM. Finally, a series of two fully connected layers with a sigmoid output activation function yields a probabilistic score which represents the likelihood of a newsworthy flood occurring in the study region during the following 24 hours. As the labels are highly skewed towards negatives, we up-sampled positive samples to constitute 20% of the training data. Hence, the resulting output is an uncalibrated score that cannot directly be interpreted as a probability for a flood to occur. Figure 4 illustrates the model architecture, and Extended Data Table 1 describes the architectural hyperparameters in more detail.

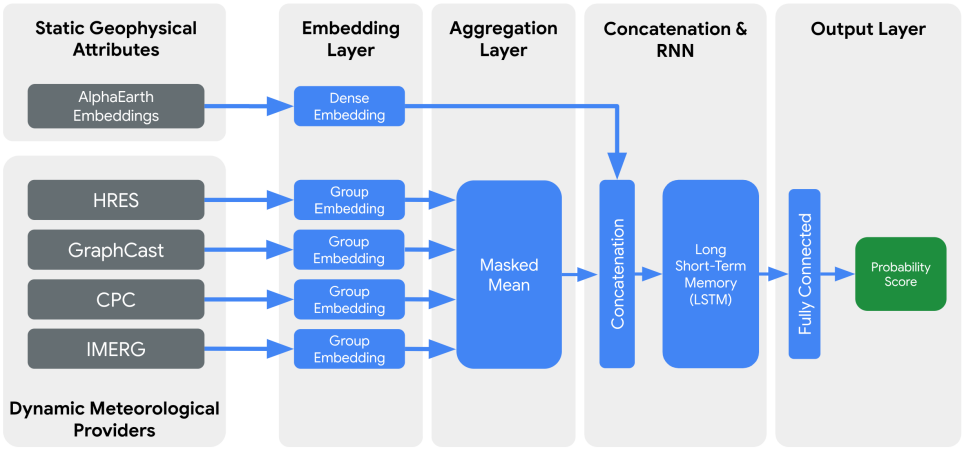

Figure 4: The architecture of the AI model presented in this manuscript.

The training objective was a binary cross-entropy loss between the predicted probability and the observed flood labels from Groundsource events. We focus on areas with a population density exceeding 100 people per km^2. This ensures sufficient media coverage to provide training and evaluation data, while prioritizing human impact: the covered area accounts for approximately 88% of the world's population, based on WorldPop data[23]. Figure 5 shows a map of the resulting spatial coverage.

Input data

We use embeddings from AlphaEarth Foundations[24] as static attributes that let the model adapt its timeseries processing to the characteristics of individual regions. AlphaEarth is a geospatial foundation model that generates 64-dimensional, 10-meter resolution embeddings from multimodal Earth observation data, including optical, radar, and climate sources. We extracted the embeddings from 2020 and spatially average their values for each prediction area. Our meteorological forcings come from the following providers:

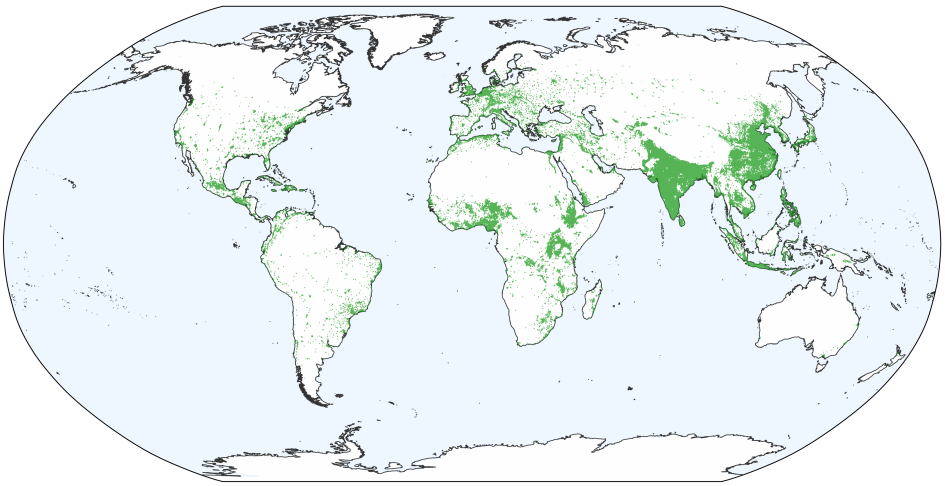

Figure 5: World map with the areas that the AI model is trained to predict highlighted in green. These correspond to areas with population density above 100 people per km^2, which cover approximately 88% of the world's population. Note that the real-time operational system excludes some of the highlighted areas due to legal restrictions.

- Single-level forecasts from the ECMWF Integrated Forecast System (IFS) High Resolution (HRES) atmospheric model[25]. The variables we use are: total precipitation (TP), 2m temperature (T2M), surface net solar radiation (SSR), surface net thermal radiation (STR), snowfall (SF), and surface pressure (SP).

- Single-level precipitation forecasts from GraphCast[26], a machine learning-based global weather forecasting system that predicts meteorological variables at a 0.25° resolution.

- Precipitation estimates from the National Oceanic and Atmospheric Administration (NOAA) Climate Prediction Center (CPC) Global Unified Gauge-Based Analysis of Daily Precipitation[27].

- Precipitation estimates from the NASA Integrated Multi-satellite Retrievals for GPM (IMERG V07) early run[28].

All input data are area-weighted averages over the $0.2° \times 0.2°$ study regions, cropped to a low-resolution map of the landmasses. Similarly, we calculate the maximum precipitation value of the providers CPC, IMERG, and GraphCast in each study region for each hour.

Target and evaluation data

Ground-truth targets for flood events stem from the Groundsource dataset, a global repository of historical flood events extracted from over 5 million publicly available news articles. Groundsource uses natural language processing to structure arbitrary textual reports into spatial polygons and temporal intervals at a daily resolution. As additional processing, we limit the duration of flood events to 3 days, and define events without an end date to last one day.

Our training and evaluation data ranges from 2018 to 2025, which covers around 78% of the events in Groundsource. We chose this cutoff, as the dataset's recency bias would likely lead to larger gaps and geographical biases for earlier periods. Given this period, we trained and evaluated the model in a k-fold temporal cross-validation setting. The years 2018–2020 were always in the training set, while each of the subsequent years represented the evaluation split in one of the folds. In total, we therefore evaluated five years of data (2021–2025).

Spatial cross-validation

To rigorously evaluate geographic generalization for the multi-country analysis (Figure 1), we employed a leave-one-country-out spatial cross-validation strategy. For each of the five countries, we trained a separate instance of the model where we excluded all data originating from within that country's borders from the training set. We then evaluated these zero-shot models on the held-out country to generate the zero-shot precision–recall curves.

Metrics and public alerts baselines

To evaluate whether AI-driven forecasting can reach operational standards, we benchmarked our system against the public flood alerts of several national expert systems. Specifically, we used baseline alerts from the United States (NWS Flood and Flash Flood Warnings), Brazil (Instituto Nacional de Meteorologia, INMET, and Centro Nacional de Gerenciamento de Riscos e Desastres, CENAD), the United Kingdom (Department for Environment Historic Flood Warnings), and Taiwan (Center for Disaster Prevention and Relief Information Platform for Public Warnings; Extended Data Figure 6). We sourced these warnings through Google's internal Public Alerts infrastructure (`https://support.google.com/publicalerts`), which aggregates warnings directly from the respective national meteorological and warning agencies. The data availability section provides details for how to access these data sets. South Africa and the Philippines are not part of this baseline comparison due to a lack of available public alert data.

For a consistent comparison, we aggregated all local alert data to match the model's $0.2^\circ \times 0.2^\circ$ grid and 24-hour forecast window. This alignment is required to ensure a consistent global evaluation: because the Groundsource data relies on (often geopolitical) boundaries extracted from text rather than exact hydrological inundation extents, the 0.2° grid serves as a common denominator. This ensures an apples-to-apples evaluation framework across diverse national systems and standardizes heterogeneous local alert formats against a unified global ground truth. Notably, given the way we define true and false alerts, this aggregation scheme does not hurt the performance of baselines with higher spatial resolution. In fact, most public alerts cover areas that are much larger than one pixel: The average alert area is 27,993 km^2 (median: 928 km^2), compared to an average pixel area of 423 km^2 (median: 441 km^2).

Following the framing of flood event prediction as a classification problem, we evaluated our system and the public alerts by means of precision and recall. A challenging aspect of this evaluation strategy is that news reports of flood events only give a fuzzy picture of the events' spatial extents. Typically, the extracted extent in Groundsource is larger than the actual flooded area, as flooding rarely follows the geopolitical boundaries that are used in textual descriptions. To account for these uncertainties, we define precision and recall as follows:

Precision Intuitively, precision measures the percentage of alerted areas that can be corroborated by an event in the ground truth. We define a positive prediction at a modeled pixel as a true positive if an event non-negligibly intersects the pixel's geometry within the same time frame. The intersection of an event and a pixel is non-negligible if it comprises at least 40% of the event area or of the pixel area. This dual condition ensures that the coarse grid does not erase highly localized floods or flood warnings. Even if a small-scale event covers only a minor fraction of a pixel, it registers as a valid intersection as long as the pixel encapsulates a significant portion of the event itself. Conversely, we only consider predictions that do not intersect with an event at all as false positives.

Recall We consider an event as recalled if a pixel that has a non-negligible intersection with the event (as defined above) issued a warning at the beginning of the day during which the event started. Further, in line with the recall definition in the Groundsource paper[13], we used events from GDACS as the ground truth for this analysis. Because GDACS focuses on significant events, evaluating recall on this source of ground truth lets us ascertain that

the models correctly alert on impactful floods. To avoid meaningless polygons, we only considered GDACS events up to a size of 50,000 km^2. For comparison, we present results that derive recall on Groundsource instead of GDACS events in Extended Data Figure 6.

We report further metrics according to their standard definitions, specifically, F1 and Critical Success Index (CSI)[29] scores, as well as the area under the precision–recall curve (AUPRC).

Data availability

Input data can be obtained from the following sources: NASA IMERG precipitation data, `https://gpm.nasa.gov/data`; ECMWF HRES forecast data, `https://www.ecmwf.int/en/forecasts/datasets/set-i`; NOAA CPC Global Unified Gauge-Based Analysis of Daily Precipitation data, `https://psl.noaa.gov/data/gridded/data.cpc.globalprecip.html`; AlphaEarth Foundations embedding data, `https://developers.google.com/earth-engine/datasets/catalog/GOOGLE_SATELLITE_EMBEDDING_V1_ANNUAL`.

Groundsource data used for training and evaluation can be obtained from `https://doi.org/10.5281/zenodo.18647053`[30]. GDACS data is available at `https://gdacs.org/`[16].

We sourced the baseline public flood alerts for the evaluated countries from Google's internal Public Alerts infrastructure, which aggregates warnings directly from the respective national agencies. Due to the proprietary nature of the aggregation infrastructure and licensing agreements with the originating agencies, we cannot directly redistribute this raw baseline data. However, the original warnings are the intellectual property of the respective national agencies and can be obtained from their websites: NWS warnings are accessible via the Iowa Environmental Mesonet (`https://mesonet.agron.iastate.edu/`); U.K. warnings are accessible via the Department of Environment Data Services Platform (`https://environment.data.gov.uk/dataset/88bed270-d465-11e4-8669-f0def148f590`); Brazil warnings via the INMET (`https://bdmep.inmet.gov.br/`) and CENAD (`https://s2id.mi.gov.br/paginas/series/`) websites; Taiwan warnings via the Information Platform for Public Warnings at the Center for Disaster Prevention and Relief (`https://alerts.ncdr.nat.gov.tw/web/`). Further instructions for the download of GDACS and public alerts data are available with our released code.

Code availability

The code to reproduce all figures and analyses reported in this paper, as well as all trained models in runnable format, are available at `https://doi.org/10.5281/zenodo.19334973`[31].

Acknowledgments

We would like to thank the NWS Forecast Office in Salt Lake City, Utah, for insights into their operational flash flood forecasting system.

Author contributions

OZ designed the model. OZ and IZ conducted the core research for the project. GN and SV contributed to the initial research regarding the utility and requirements of an operational flash flood forecasting system. HF and GL contributed to the design of the operational system, which was then implemented by RM, HF, AN, and IZ. OZ, MG, and DC drafted the manuscript. All authors contributed to the critical revision of the manuscript and approved the final submitted version. During the preparation of this work, the authors used Gemini to edit and improve the

readability of the manuscript. After using this tool, the authors reviewed and edited the content as needed. The authors take full responsibility for the content of the publication.

Competing interests

The authors declare no competing interests.

References

[1] World Meteorological Organization. 2021 state of climate services: Water. Tech. Rep. WMO-No. 1278, World Meteorological Organization, Geneva, Switzerland (2021).

[2] World Meteorological Organization. Devastating floods highlight need and challenges of warnings (2025). URL `https://wmo.int/media/news/devastating-floods-highlight-need-and-challenges-warnings`. Accessed March 30, 2026.

[3] van Loenhout, J. *et al.* The human cost of disasters: an overview of the last 20 years (2000–2019). Tech. Rep., Centre for Research on the Epidemiology of Disasters (CRED) and United Nations Office for Disaster Risk Reduction (UNDRR) (2020).

[4] Schröter, K. *et al.* Effectiveness and efficiency of early warning systems for flash-floods. *Bundesministerium für Bildung und Forschung, Minsterio de educación y ciencia, Darmstadt University of Technology-IHWP, Universitat Politècnica de Catalunya-GRAHI-UPC, University of Natural Resources and Applied Life Science (BOKU), Pro Aqua-Water & Finance: London, UK* (2008).

[5] World Meteorological Organization. WMO guidelines on multi-hazard impact-based forecast and warning services. Tech. Rep. WMO-No. 1150, World Meteorological Organization, Geneva, Switzerland (2015).

[6] United Nations Office for Disaster Risk Reduction. Sendai framework for disaster risk reduction 2015-2030. Tech. Rep., UNDRR, Geneva, Switzerland (2015).

[7] United Nations Office for Disaster Risk Reduction & World Meteorological Organization. Global status of multi-hazard early warning systems (2025). Tech. Rep., UNDRR and WMO, Geneva, Switzerland (2025).

[8] Acosta-Coll, M., Ballester-Merelo, F., Martinez-Peiró, M. & De la Hoz-Franco, E. Real-time early warning system design for pluvial flash floods—a review. *Sensors* **18**, 2255 (2018).

[9] Georgakakos, K. P. Analytical results for operational flash flood guidance. *Journal of Hydrology* **317**, 81–103 (2006).

[10] Carpenter, T. M., Sperfslage, J. A., Georgakakos, K. P., Sweeney, T. & Fread, D. L. National threshold runoff estimation utilizing GIS in support of operational flash flood warning systems. *Journal of Hydrology* **224**, 21–44 (1999).

[11] Raynaud, D. *et al.* A dynamic runoff co-efficient to improve flash flood early warning in Europe: evaluation on the 2013 central European floods in Germany. *Meteorological Applications* **22**, 410–418 (2015).

[12] Van Der Knijff, J. M., Younis, J. & De Roo, A. P. J. LISFLOOD: a GIS-based distributed model for river basin scale water balance and flood simulation. *International Journal of Geographical Information Science* **24**, 189–212 (2010).

[13] Mayo, R. *et al.* Groundsource: A dataset of flood events from news. *preprint* (2026).

[14] Comanici, G. *et al.* Gemini 2.5: Pushing the frontier with advanced reasoning, multimodality, long context, and next generation agentic capabilities. *arXiv:2507.06261* (2025).

[15] Nearing, G. *et al.* Global prediction of extreme floods in ungauged watersheds. *Nature* **627**, 559–563 (2024).

[16] Masante, D. *et al.* Multi-hazard early warning system Global Disaster Alert and Coordination System (GDACS). Tech. Rep., European Commission: Joint Research Centre (2025).

[17] Nearing, G. *et al.* Comment on "when are AI models ready for deployment? reassessing Google's global AI flood forecasting system through the lens of responsible modelling" (2024). URL `https://doi.org/10.5281/zenodo.19023834`.

[18] Zscheischler, J. *et al.* A typology of compound weather and climate events. *Nature reviews earth & environment* **1**, 333–347 (2020).

[19] Hochreiter, S. & Schmidhuber, J. Long short-term memory. *Neural Computation* **9**, 1735–1780 (1997).

[20] Kratzert, F. *et al.* Towards learning universal, regional, and local hydrological behaviors via machine learning applied to large-sample datasets. *Hydrology and Earth System Sciences* **23**, 5089–5110 (2019).

[21] Mai, J. *et al.* The Great Lakes runoff intercomparison project phase 4: the Great Lakes (GRIP-GL). *Hydrology and Earth System Sciences* **26**, 3537–3572 (2022).

[22] Gauch, M. *et al.* How to deal w___ missing input data. *Hydrology and Earth System Sciences* **29**, 6221–6235 (2025).

[23] WorldPop Authors. WorldPop (2026). URL `https://www.worldpop.org/`. Accessed: March 30, 2026.

[24] Brown, C. F. *et al.* AlphaEarth foundations: An embedding field model for accurate and efficient global mapping from sparse label data. *arXiv:2507.22291* (2025).

[25] ECMWF. *IFS Documentation*. European Centre for Medium-Range Weather Forecasts, Reading, U.K. (2023). URL `https://www.ecmwf.int/en/publications/ifs-documentation`. Accessed: March 30, 2026.

[26] Lam, R. *et al.* Learning skillful medium-range global weather forecasting. *Science* **382**, 1416–1421 (2023).

[27] Chen, M. *et al.* Assessing objective techniques for gauge-based analyses of global daily precipitation. *Journal of Geophysical Research: Atmospheres* **113** (2008).

[28] Huffman, G. J. *et al.* *Integrated Multi-satellite Retrievals for the Global Precipitation Measurement (GPM) Mission (IMERG)*, 343–353 (Springer International Publishing, Cham, 2020).

[29] Schaefer, J. T. The Critical Success Index as an indicator of warning skill. *Weather and Forecasting* **5**, 570–575 (1990).

[30] Mayo, R. *et al.* Groundsource: A dataset of flood events from news (data) (2026). URL `https://doi.org/10.5281/zenodo.18647054`.

[31] Zlydenko, O. *et al.* AI learns to forecast global flood events from historical news (code and data) (2026). URL `https://doi.org/10.5281/zenodo.19334973`.

Extended Data figures and tables

Hyperparameters

Table 1 lists the hyperparameters of the architecture used in the AI model.

Table 1: Model hyperparameters.

Hyperparameter	Value
Activation	ReLU
Output activation	Sigmoid
Attribute embedding layers	[32, 16, 4]
Forcing embedding layers	[16, 16]
Fully connected head layers	[16, 1]
LSTM hidden size	128
L2 regularization	3e-4
Initial learning rate	3e-5
Learning rate schedule	Exponential decay with decay rate of 0.999 every 500 steps
Batch size	256
Epochs	40
Update steps per epoch	1500

Full tables of metrics and sample sizes

Table 2 details the area under the precision–recall curve (AUPRC), Critical Success Index (CSI), and F1 scores for the different models evaluated in the paper. Further, Table 3 provides an overview of the sample sizes used to calculate all statistics. Most metrics were calculated based on both Groundsource events (for precision; in Figure 6 also for recall) and on GDACS events (for recall). We therefore report both numbers in the table.

Table 2: AUPRC, CSI, and F1 scores for the AI model, the AI model under zero-shot evaluation (removing the evaluated country from the training set), and the local expert system alerts. CSI and F1 scores for the AI models are calculated using a classification threshold of 0.74, which optimizes the F1 score globally. The local alerts are binary and therefore do not have an AUPRC metric. For the U.S., local alerts refer to the union of NWS Flood and Flash Flood Warnings.

	AUPRC		CSI			F1		
	Globally trained	Zero-shot	Globally trained	Zero-shot	Local alerts	Globally trained	Zero-shot	Local alerts
U.S.	0.22	0.15	0.16	0.12	0.14	0.32	0.23	0.28
Brazil	0.33	0.26	0.17	0.11	0.06	0.34	0.21	0.10
U.K.	0.30	0.26	0.19	0.09	0.16	0.37	0.30	0.29
South Africa	0.25	0.21	0.15	0.14	–	0.33	0.26	–
Philippines	0.21	0.19	0.18	0.16	–	0.31	0.26	–
Global	0.23	–	0.18	–	–	0.30	–	–

Table 3: Number of considered Groundsource and GDACS events in each hold-out country and globally during each evaluation year.

	Groundsource	GDACS
U.S.	107,779	96
Brazil	94,293	53
U.K.	32,116	64
South Africa	4,567	43
Philippines	15,266	89
Taiwan	9,300	–
Global, 2021	218,994	472
Global, 2022	225,068	583
Global, 2023	261,813	691
Global, 2024	395,506	729
Global, 2025	402,012	745
Global, all years	1,503,393	3,220

Groundsource recall

Figure 6 replicates Figure 1 from the main paper but uses Groundsource events as the ground truth for the recall calculation. The trade-off is that GDACS events ensure coverage of high-impact events at a very low rate of false reports, while Groundsource ensures high overall coverage at the expense of more misreported events.

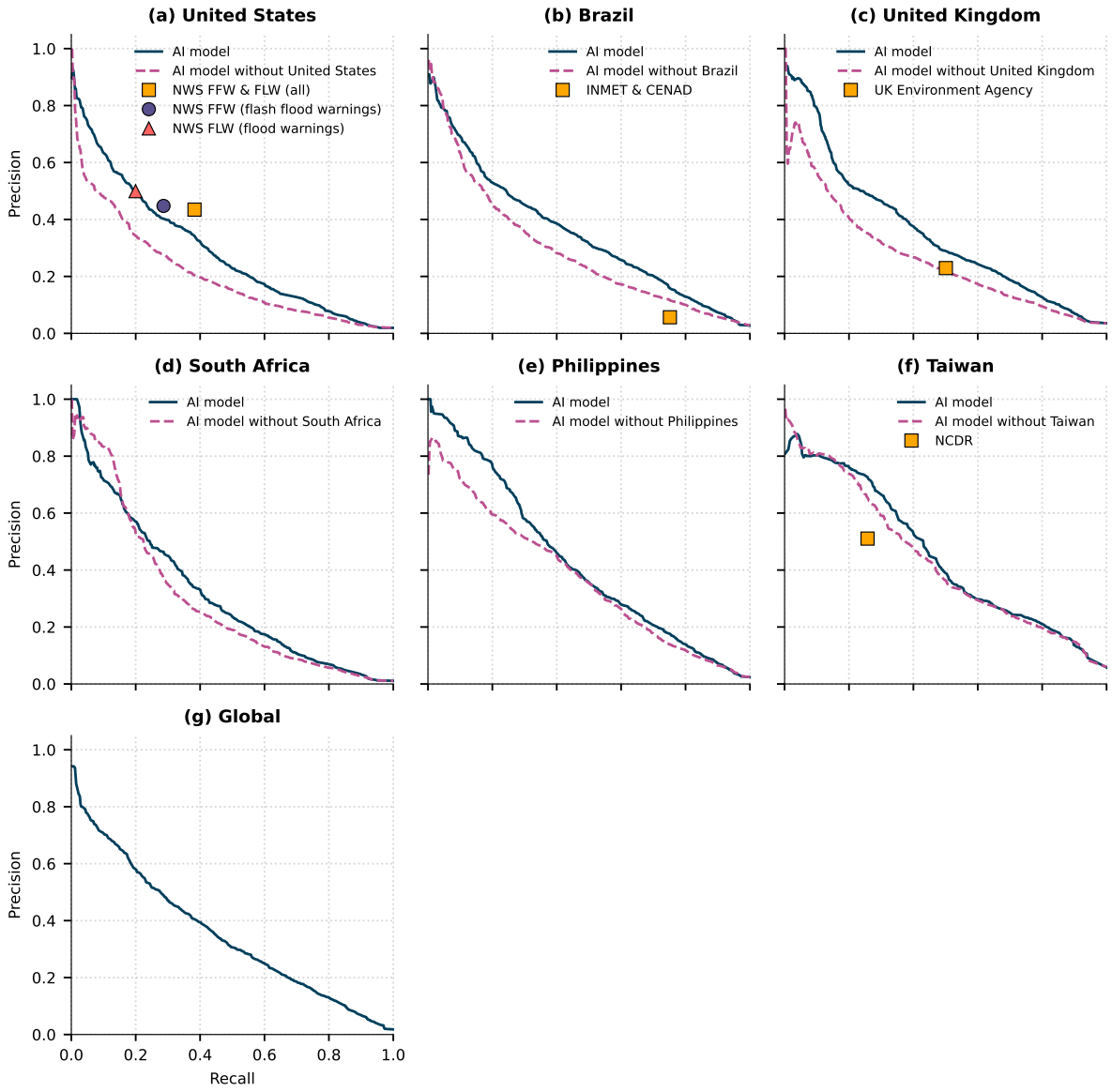

Figure 6: Same as Figure 1, but using Groundsource events as the ground truth for recall calculation. For efficient calculation, we approximate the recall on 500 randomly chosen events in each plot. Extending Figure 1, this plot adds data for Taiwan, which has no GDACS events in the evaluation period.